Resonant Behavior and Selective Switching of Stop Bands in Three-Dimensional Photonic Crystals with Inhomogeneous Components

A. V. Baryshev,[1,2] A. B. Khanikaev,[1] M. Inoue,[1] P. B. Lim,[1] A. V. Sel'kin,[1,2] G. Yushin,[3] and M. F. Limonov[1,2]

[1]*Toyohashi University of Technology, Toyohashi, Aichi 441-8580, Japan*

[2]*Ioffe Physico-Technical Institute, St. Petersburg 194021, Russia*

[3]*School of Materials Science and Engineering, Georgia Institute of Technology, Atlanta, Georgia 30332-0245, USA*

(Received 20 February 2007; published 8 August 2007)

We demonstrate that, in contrast with the well-studied photonic crystals consisting of two homogeneous components, photonic crystals comprised of inhomogeneous or multiple (three or more) components may bring new opportunities to photonics due to the discovered quasiperiodic resonant behavior of their (*hkl*) stop bands as a function of the reciprocal lattice vector. A resonant stop band cannot be switched off for any permittivity of structural components. Tuning the permittivity or structural parameters allows the selective on-off switching of nonresonant (*hkl*) stop bands. This independent manipulation of light at different Bragg wavelengths provides a new degree of freedom to design selective optical switches and waveguides. Transmission experiments performed on synthetic opals confirmed the theoretical predictions.

DOI: 10.1103/PhysRevLett.99.063906 PACS numbers: 42.70.Qs, 42.25.Fx, 42.79.Fm

Photons, as the quickest messengers of information, are predicted to replace electrons in future telecommunication circuits, and photonic crystals (PCs) may play a decisive role in this revolution. Although much effort has been made to fabricate and study different kinds of artificial PCs, i.e., structures with the spatial modulation of the permittivity, most PCs consist of two homogeneous materials [1,2] and could be called two-component PCs (TCPCs). TCPCs become fully transparent when the permittivity of the first component matches the permittivity of the second component [3]. In this case, all of the (*hkl*) photonic stop bands, defined as wavelength ranges where Bragg conditions cause diffraction from the (*hkl*) planes, would disappear since the nondiffraction conditions would be fulfilled for all of the (*hkl*) crystallographic planes simultaneously. Thus, TCPCs do not permit selective control over information transmitted using different Bragg wavelengths $\lambda_{(hkl)}$.

In this Letter, in order to design a novel PC that does not have such a limitation, we studied the photonic band structure of photonic crystals with inhomogeneous components (PCWICs) and discovered new effects which an inhomogeneous nature of a component brings about. We considered the nondiffraction condition for a PCWIC consisting of the spheres with an arbitrary spherically symmetrical profile of the permittivity $\varepsilon_s(r)$, when the space between spheres is filled with a homogeneous filler of the permittivity ϵ_f. We calculated the photonic band structure and transmission spectra using the photonic Korringa-Kohn-Rostocker method [4] and the plane wave expansion technique [5,6]. We also developed an analytical approach to demonstrate how the nondiffraction regime is associated with the reciprocal lattice vector $\mathbf{G}$ when the structural inhomogeneity of the spheres is taken into account. The results and conclusions based on all three methods are very similar. Here we present and discuss only the latter one, which demonstrates clearly that PCWICs exhibit quasiperiodic resonant behavior of their (*hkl*) stop bands with the opportunity to separately switch them on and off and, thus, simultaneously and independently manipulate light at various Bragg wavelengths. Theoretical results and data of transmission experiments performed on synthetic opals showed excellent agreement.

Intensity of the Bragg diffraction from a certain (*hkl*) family of crystal planes is governed by the scattering form factor $S(\mathbf{G}_{hkl})$ [7]. Therefore, the nondiffraction regime is realized when a condition of vanishing the scattering form factor is satisfied:

$$S(\mathbf{G}_{hkl}) \equiv \int_{V_0} d\mathbf{r}\left(\frac{1}{\varepsilon_s(r)} - \frac{1}{\varepsilon_f}\right)\Theta(r_s - r)\exp(-i\mathbf{G}_{hkl}\cdot\mathbf{r}) = 0, \quad (|\mathbf{G}|_{hkl} \neq 0), \tag{1}$$

where $\mathbf{G}_{hkl}$ is the reciprocal lattice vector which uniquely determines the corresponding $\{hkl\}$ family of crystal planes, V_0 is the volume of the unit cell in a PC, r_s is the radius of the sphere with the spherically symmetrical permittivity profile $\varepsilon_s(r)$, and $\Theta(x)$ is the unit step function so that $\Theta(x) = 1$ for $x \geq 0$ and zero for $x < 0$. However, one should be careful with usage of the condition (1) in the case of the multiple Bragg diffraction regime, when stop bands corresponding to different $\mathbf{G}_{hkl}$ overlap. In this case, a nondiffraction condition should be obtained by solving the full eigenvalue problem [8]. Otherwise, Eq. (1) corresponds to the disappearance of an (*hkl*) stop band. After the integration over angular variables in the spherical coordinate system, we can obtain the value of the filler permittivity $\varepsilon_f^0(G_{hkl})$ that meets the nondiffraction regime:

$$\varepsilon_f^0(G_{hkl}) = \frac{\frac{1}{G_{hkl}^2}[\sin(G_{hkl}r_s) - G_{hkl}r_s\cos(G_{hkl}r_s)]}{\int_0^{r_s}\frac{r}{\varepsilon_s(r)}\sin(G_{hkl}r)dr}. \tag{2}$$

In all subsequent calculations, we consider ε_f^0 to be a continuous function of $G = G_{hkl} = |\mathbf{G}_{hkl}|$ and omit the hkl indices. In the case of the TCPC [homogeneous spheres: $\varepsilon_s(r) = \varepsilon_s = \text{const}$], after the integration in the denominator of Eq. (2), we obtain the obvious condition $\varepsilon_f^0 = \varepsilon_s$, which means the lack of diffraction from all of the (hkl) families of crystal planes at the same value of the filler permittivity.

To study the general features of stop-band formation in a PCWIC, we considered the nondiffraction conditions for various crystal structures and permittivity profiles $\varepsilon_s(r)$ in a large range of G. Figure 1 shows an example of such calculations for the closed-packed fcc lattices consisting of spheres with different $\varepsilon_s(r)$ functions. Our studies revealed a number of unexpected results. First, any inhomogeneity within the sphere results in a variation of ε_f^0 depending on G, i.e., in a variation of the nondiffraction condition for different (hkl) photonic stop bands. Second, all of the dependencies $\varepsilon_f^0(G)$ demonstrate quasiperiodic behavior with prominent resonance features at $G = G_{\text{res}}$. The quasiperiod of $\varepsilon_f^0(G)$ is determined by vanishing the denominator of Eq. (2). At the resonance, the nondiffraction condition is not fulfilled at any profile of $\epsilon_s(r)$ and filler permittivity ϵ_f. Away from the resonance for any $G \neq G_{\text{res}}$ and any physically reasonable permittivity profile of spheres $\epsilon_s(r)$, one can find a filling medium with permittivity $\varepsilon_f^0(G)$ providing for suppressing the (hkl) stop band

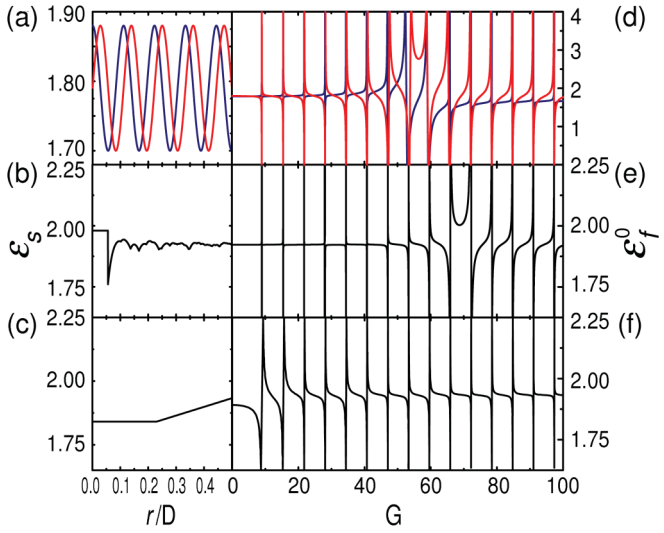

FIG. 1 (color). Resonant behavior of the nondiffraction conditions in PCWICs. The lattice consists of the spheres with inhomogeneous profiles $\varepsilon_s(r)$ (a)–(c) and homogenous filler ε_f. The modeling profiles of the sphere permittivity $\varepsilon_s(r)$: $\varepsilon_s(r) = \varepsilon_s(0) + \Delta\varepsilon \sin(ar)$ (red) and $\varepsilon_s(r) = \varepsilon_s(0) + \Delta\varepsilon \cos(ar)$ (blue) (a), averaged over spherical angle permittivity of the sphere composed of close-packed small spheres (b), an increasing piecewise-linear function (c). (d)–(f) Filler permittivity $\varepsilon_f^0(\mathbf{G})$ of nondiffraction condition for different $\varepsilon_s(r)$ corresponding to (a)–(c). The quasiperiodic character of the $\varepsilon_f^0(\mathbf{G})$ functions with strong resonances is clearly seen.

so that the resultant PC becomes optically transparent at the Bragg wavelength $\lambda_{(hkl)}$.

To verify the theoretical predictions experimentally, we chose synthetic opals as 3D PC model objects [9–19]. Opals consist of a-SiO_2 silica spheres several hundred nanometers in diameter arranged into the close-packed fcc structure. Amorphous silica mixed with other minerals generally fills interstices in natural opals [20]. Liquid or solid fillers having controlled permittivity values are used in synthetic opals [9,14,16–19]. The a-SiO_2 spheres are not homogeneous [21,22]. Our studies of the a-SiO_2 spheres unambiguously confirmed their complicated structure with a porous core and a dense near-surface region (Fig. 2). [The scanning and transmission electron microscopy (SEM and TEM, respectively) was performed using an FEI XL30 environmental field emission SEM and JOEL 2010 F field emission TEM microscopes, respectively.] Thus, we hypothesized that opals could be considered as PCWICs, in contrast to a long-held axiom that the sphere superstructure was not essential for optical properties [17,19,23]. Below, we demonstrate various (hkl) photonic stop bands in opals to appear and disappear at significantly different filler permittivity, confirming the theoretical predictions for PCWICs.

The most appropriate way to detect the modification of different (hkl) stop bands with variation of the dielectric contrast is transmission experiments. The high quality synthetic opal samples [17–19] allowed us to measure angle-resolved polarized transmission spectra for any direction of the wave vector $\mathbf{k}$ in the Brillouin zone (BZ) of the fcc opal lattice. We investigated two samples of a-SiO_2 spheres 290 ± 15 and 315 ± 15 nm in diameter using a Shimadzu UV-3100 spectrophotometer over the spectral range of 365–825 nm for linear polarizations parallel ($E_{||}$) and perpendicular ($E_{\perp}$) to the scanning planes. The chosen diameters of spheres and investigated spectral range allowed us to analyze the {111}, {200}, and {220} photonic stop bands (for experimental details and assignment of the stop bands, see [18,24,25]). By analyzing the collected experimental data, we found that all of the results we report here are reproducible and are not specific to a sample or method. Hereafter, we discuss the results obtained for the sample of ~315 nm spheres.

The results of the immersion spectroscopy of opals (Fig. 3) show how variation in the filler permittivity causes

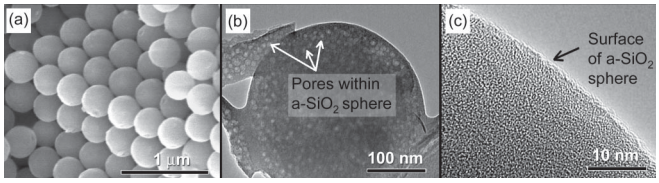

FIG. 2. (a) SEM and (b),(c) TEM micrographs of the investigated opals. Fcc-packed silica spheres show a smooth dense surface and a porous internal structure. The sample was studied without coating.

changes in the intensity and linewidth of transmission dips. Clearly, the dependencies of the {111}, {022}, and {020} stop-band parameters on the dielectric contrast are different, and various (hkl) stop bands disappear in the transmission spectra at notably different values of the filler permittivity ϵ_f. The (111) stop band dramatically weakens and practically disappears at the filler permittivity $\varepsilon_f^0(G_{111}) = 1.83$, when the sample becomes optically transparent at the Bragg wavelength $\lambda_{(111)}$ (~ 710 nm for the L point and ~ 570 nm for the K point of the BZ); see Figs. 3(a) and 3(b). In contrast, at $\epsilon_f = 1.83$, the {020} and {022} bands are well defined. The (022) stop band disappears at the significantly higher filler permittivity $\varepsilon_f^0(G_{022}) = 1.92$, when the sample becomes optically transparent at the Bragg wavelength $\lambda_{(022)}$ (~ 430 nm for the K point) while both the {111} and the {020} bands exist [Fig. 3(b)]. Moreover, the dip associated with the (020) stop band demonstrates absolutely different behavior: the stop band exists at all investigated fillers with permittivity ranging from 1.76 to 1.99 (methanol-ethanol and water-glycerol solutions) [Fig. 3(c)]. The dependencies observed (Fig. 3) clearly indicate a breakdown of the commonly accepted two-component model of opals. Indeed, the splitting of the $\varepsilon_f^0(G_{hkl})$ values for different (hkl) stop bands is not compatible with the two-component model of PCs.

The smooth and continuous surface of a-SiO_2 spheres indicates higher density of a near-surface region of the spheres as compared with the porous core; see Figs. 2(a) and 2(b). Therefore, to understand how this fact can be manifested experimentally, we simulated the permittivity profile $\varepsilon_s(r)$ by an increasing piecewise-linear function (red line in the inset in Fig. 4). The obtained results (red line, Fig. 4) are in excellent agreement with the experimental data (Fig. 3). Such a permittivity profile results in $\varepsilon_f^0(G_{111}) < \varepsilon_f^0(G_{022})$. By tuning slightly the parameters of the $\varepsilon_s(r)$ function, we can easily obtain the experimentally observed values $\varepsilon_f^0(G_{111}) = 1.83$ and $\varepsilon_f^0(G_{022}) = 1.92$. The proximity of the reciprocal lattice vector modulus $G_{200} = 8.886D^{-1}$ to the resonant value $G_{\text{res}} \sim 8.9D^{-1}$ is responsible for the experimentally observed stop band at any value of ε_f. For comparison, Fig. 4 also shows the conditions for the disappearance of stop bands in the case when $\varepsilon_s(r)$ follows a decreasing piecewise-linear function (green line, Fig. 4) and a profile of the sphere comprising close-packed small-size spheres (blue line, Fig. 4). The former (green line in the inset in Fig. 4) results in $\varepsilon_f^0(G_{111}) > \varepsilon_f^0(G_{022})$, and the latter (blue line in the inset in Fig. 4) does not provide a remarkable difference between $\varepsilon_f^0(G_{111})$ and $\varepsilon_f^0(G_{022})$, thus contradicting experimental observations.

In the future era of all-optical communication networks, PCWICs will be increasing in importance due to their variety of functions governed by the selective on-off switching effect. Figure 5 demonstrates effect of the inhomogeneous nature of one component of PCs on their {hkl} stop bands states. Conventional TCPC can exist only in two states—either all of its stop bands are open

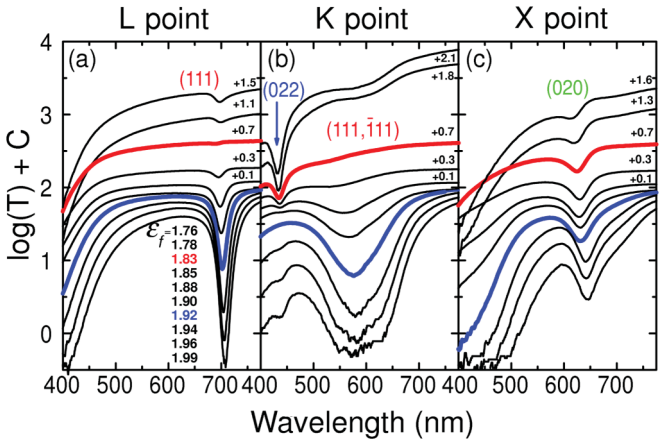

FIG. 3 (color). Transmission spectra of an opal sample (~ 315-nm a-SiO_2 spheres) as a function of the permittivity of the filler ε_f for (a) $\Gamma \rightarrow L$, (b) $\Gamma \rightarrow K$, and (c) $\Gamma \rightarrow X$ incidence. The column of numbers in (a) presents the values of ε_f for corresponding transmission spectra in (a)–(c) from top to bottom. The curves are shifted vertically by the values shown. The spectra obtained for the filler with $\varepsilon_f = 1.83$ are marked by red and for the filler with $\varepsilon_f = 1.92$ by blue.

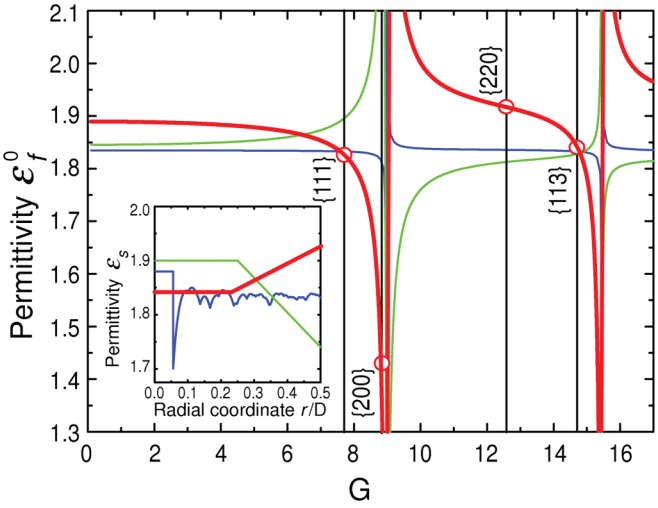

FIG. 4 (color). Nondiffraction conditions for an opal structure. The filler permittivity $\varepsilon_f^0(\mathbf{G})$ of the nondiffraction regime as a function on the reciprocal lattice vector calculated from Eq. (2) for different profiles $\varepsilon_s(r)$ simulating the a-SiO_2 spheres of synthetic opals. The profiles $\varepsilon_s(r)$ are drawn in the inset. The modulus of the shortest reciprocal lattice vectors of the fcc structure $G\{111\} = 7.695D^{-1}$, $G\{200\} = 8.886D^{-1}$, $G\{220\} = 12.566D^{-1}$, and $G\{113\} = 14.735D^{-1}$ are shown by the vertical lines, $G\{hkl\} = \pi D^{-1}\sqrt{2(h^2 + l^2 + k^2)}$. For all of the profiles, $G\{200\}$ is located near the first resonance. Piecewise-linear profile $\varepsilon_s(r)$ with a denser near-surface region (red) gives the values $\varepsilon_f^0(111) = 1.83$, $\varepsilon_f^0(220) = 1.91$, and $\varepsilon_f^0(200) = 1.43$ and provides excellent agreement with the experimental nondiffraction values of ε_f^0.

(a)

TCPC	State 1 $\varepsilon_f \neq \varepsilon_s$	State 2 $\varepsilon_f = \varepsilon_s$
Stop-Bands $\{hkl\}, \lambda_{(hkl)}$	OFF	ON

(b)

PCwIC	State 1 $\varepsilon_f = 2.0$	State 2 $\varepsilon_f = 1.92$	State 3 $\varepsilon_f = 1.83$	State 4 $\varepsilon_f = 1.45$
Stop-Band {111}, $\lambda_{(111)}$	OFF	OFF	ON	OFF
Stop-Band {200}, $\lambda_{(200)}$	OFF	OFF	OFF	ON
Stop-Band {220}, $\lambda_{(220)}$	OFF	ON	OFF	OFF
Stop-Band {113}, $\lambda_{(113)}$	OFF	OFF	ON	OFF

FIG. 5 (color). (a) An optical switch based on conventional TCPCs. (b) A PCWIC with tunable permittivity of one component. For simplicity, only four $\{hkl\}$ stop bands are considered, and their states are shown according to the nondiffraction conditions for the above discussed fcc opal lattice (Fig. 4).

($\varepsilon_f \neq \varepsilon_s$, the nondiffraction condition is not achieved, incident beam reflected, state off) or all are closed ($\varepsilon_f = \varepsilon_s$, PC becomes completely homogeneous and transparent, state on) [Fig. 5(a)]. Therefore, TCPC does not allow independent processing of information transmitted using different Bragg wavelengths $\lambda_{(hkl)}$. In contrast, PCWICs are capable to switch on-off stop bands selectively, creating several possible states, and therefore have notably enhanced communication capabilities [Fig. 5(b)].

The on-off selective switching can be realized by tuning the permittivity of one (or several) component(s) in a PCWIC. Such a route was used, e.g., for ultrafast (femtosecond time scale) optical switching of the (111) stop band in a Si-opal composite [26]. In that work, however, the wavelength selectivity of switching was not investigated. The on-off selective switching can also be achieved using piezospectroscopy [27], i.e., by modulation of the reciprocal lattice vector G. This modulation can be particularly effective near the resonance ($G \sim G_{\text{res}}$), e.g., for Bragg wavelengths $\lambda_{(200)}$ (Fig. 4). In this case, a uniform pressure or expansion of the PC lattice will switch all of the stop bands, while a uniaxial stress will split the certain $\{hkl\}$ family, allowing selective switching of a (hkl) stop band. For example, stress along the [010] axis of an fcc lattice will switch only the (020) stop band in the {200} family, while (200) and (002) stop bands will remain unaffected (or slightly affected).

To conclude, we have theoretically predicted and experimentally confirmed the capability of PCWICs to serve as optical switches or waveguides with parallel control over information transmitted at different optical frequencies. This independent manipulation of light provides a new degree of freedom to design a future generation of selective optical switches and waveguides. In a passive regime, PCWICs exhibit different nondiffraction conditions for various $\{hkl\}$ stop bands. During dynamic modulation of their lattice parameters or permittivity of components, PCWICs can switch light signals transmitted at certain Bragg wavelengths selectively.

We thank A. A. Kaplyanskii and V. A. Kosobukin for helpful discussions, M. I. Samoylovich and A. V. Guryanov for providing us with the opal samples, and V. G. Golubev and S. F. Kaplan for preparation of the opal film for SEM measurements. SEM was performed in the Centralized Materials Characterization Facility of A. J. Drexel Nanotechnology Institute. TEM studies were done in Penn Regional Nanotechnology Facility, University of Pennsylvania. This work was supported in part by the super optical information memory project by MEXT, Grant-in-Aid for Scientific Research from JSPS, Japan, and by the RFBR, Russia, Grant No. 05-02-17809.

[1] S. G. Johnson and J. D. Joannopoulos, *Photonic Crystals: The Road from Theory to Practice* (Kluwer Academic, Boston, 2003).
[2] K. Inoue and K. Ohtaka, *Photonic Crystals: Physics, Fabrication and Applications* (Springer-Verlag, Berlin, 2004).
[3] A. Yariv and P. Yeh, *Optical Waves in Crystals* (Wiley, New York, 1984).
[4] A. Modinos, N. Stefanou, I. E. Psarobas, and V. Yannopapas, Physica (Amsterdam) **296B**, 167 (2001).
[5] H. S. Sözüer, J. W. Haus, and R. Inguva, Phys. Rev. B **45**, 13 962 (1992).
[6] K. Busch and S. John, Phys. Rev. E **58**, 3896 (1998).
[7] K. Sakoda, *Optical Properties of Photonic Crystals* (Springer, Berlin, 2005), 2nd ed.
[8] H. M. van Driel and W. L. Vos, Phys. Rev. B **62**, 9872 (2000).
[9] V. N. Astratov *et al.*, Nuovo Cimento D **17**, 1349 (1995).
[10] A. A. Zakhidov *et al.*, Science **282**, 897 (1998).
[11] A. Blanco *et al.*, Nature (London) **405**, 437 (2000).
[12] Yu. A. Vlasov, X.-Z. Bo, J. C. Sturm, and D. J. Norris, Nature (London) **414**, 289 (2001).
[13] V. N. Astratov *et al.*, Phys. Rev. B **66**, 165215 (2002).
[14] V. G. Golubev *et al.*, J. Non-Cryst. Solids **299–302**, 1062 (2002).
[15] A. F. Koenderink and W. L. Vos, Phys. Rev. Lett. **91**, 213902 (2003).
[16] C. Lopez, Adv. Mater. **15**, 1679 (2003).
[17] A. V. Baryshev *et al.*, Phys. Rev. B **70**, 113104 (2004).
[18] A. V. Baryshev *et al.*, Phys. Rev. B **73**, 033103 (2006).
[19] A. V. Baryshev *et al.*, Phys. Rev. B **73**, 205118 (2006).
[20] A. W. Ekert, *The World of Opals* (Wiley, New York, 1997).
[21] R. K. Iler, *The Chemistry of Silica* (Wiley, New York, 1979).
[22] I. A. Karpov *et al.*, Phys. Solid State **47**, 347 (2005).
[23] S. G. Romanov *et al.*, Phys. Rev. E **63**, 056603 (2001).
[24] M. V. Rybin *et al.*, Photonics Nanostruct. **4**, 146 (2006).
[25] M. V. Rybin, K. B. Samusev, and M. F. Limonov, Photonics Nanostruct. (to be published).
[26] D. A. Mazurenko *et al.*, Phys. Rev. Lett. **91**, 213903 (2003).
[27] M. Cardona, *Modulation Spectroscopy* (Academic, New York, 1969).